

# Drone-based single-shot fault detection method for wind turbines – conception and initial feasibility study

Tim Czasch<sup>a</sup> and Peter Lehmann<sup>a</sup>

<sup>a</sup>Measurement Technology Group, Faculty of Electrical Engineering and Computer Science, University of Kassel, Wilhelmshoer Allee 71, Kassel 34121, Germany

## ABSTRACT

Fringe projection profilometry (FPP) is an optical, non-contact 3D measurement method widely applied across industries. In the manufacturing industry, this method can be used to inspect structural components and detect defects such as buckles or gap sizes in automotive industries. Due to its resolution in the micrometer range, also smaller components can be measured precisely. Therefore, FPP can also be used in other areas, such as monitoring wound healing processes or deformation of brake disks. However, the usually static setup and the use of multi-step phase-shifting algorithms often limits the applicability, especially as the latter requires an interference-free system. Nevertheless, due to the large possible field of view (often several square decimeters, or even more) and the good depth resolution, the use of FPP is also interesting for inspection and fault detection of wind turbines or buildings, for example. However, as surfaces to be measured are often difficult to reach, a static setup from the ground is economically not feasible. Therefore, we present the concept of an FPP system mounted on a drone for in-flight inspection. The challenge when using a drone is due to motion sensitivity resulting in additional noise, which necessitates single-shot measurements based on the analysis of a single camera image only. Compared to conventional FPP our method projects a fixed grating and requires a complex spatially-resolved phase analysis. Although it is restricted with respect to the maximum height of steps on the surface, it promises good results in the desired applications. Initial measurement results obtained with an FPP system under laboratory conditions are presented as a feasibility analysis for drone-based investigation of rotor blades. This feasibility study aims at ensuring the basic suitability of the FPP method in the presence of typical surface coatings of rotor blades.

**Keywords:** Fringe projection profilometry, Optical 3D measurement, Drone-based, single shot, wind turbines, Phase analysis, short-time Fourier transform, Hilbert transform

## 1. MOTIVATION

Surface anomalies are the consequence of the stress and aging of technical structural components, frequently resulting in major damage.<sup>1</sup> The identification of critical surface anomalies at an early stage facilitates the implementation of targeted repair measures, thereby preventing the occurrence of significant damage or failure. Particularly in places that are difficult to access, such as tall constructions, the assessment of critical surface anomalies is currently often carried out by visual<sup>2</sup> or camera-based inspection.<sup>3</sup> Moreover, assessing severity is difficult when relying on two-dimensional image information such as that provided by a camera. Despite the utilization of three-dimensional image information, visual inspection by humans is often flawed.

In order to detect surface structures precisely and objectively, innovative measuring methods are required.<sup>4</sup> The need for efficient, non-contact and highly accurate inspection solutions is particularly important for large or difficult to access structures, such as those found in the energy or construction industries. Wind turbines are a particularly challenging and relevant application. Due to their exposed location and size, their rotor blades suffer from extreme environmental stresses.<sup>5</sup>

Rotor blades are subject to a multitude of stresses, including wind loads, temperature fluctuations, UV radiation, precipitation, hail, sand abrasion, and mechanical fatigue. The most common types of damage are

---

Further author information: (Send correspondence to Tim Czasch)

Tim Czasch: E-mail: tim.czasch@uni-kassel.de

surface erosion, delamination, cracks, fiber damage and structural failure.<sup>5-7</sup> Especially a lot of stress is placed on the leading edge, which is why abrasion and defects often occur there first. This leading edge can be seen in Fig. 1 of a 22-year-old rotor blade.

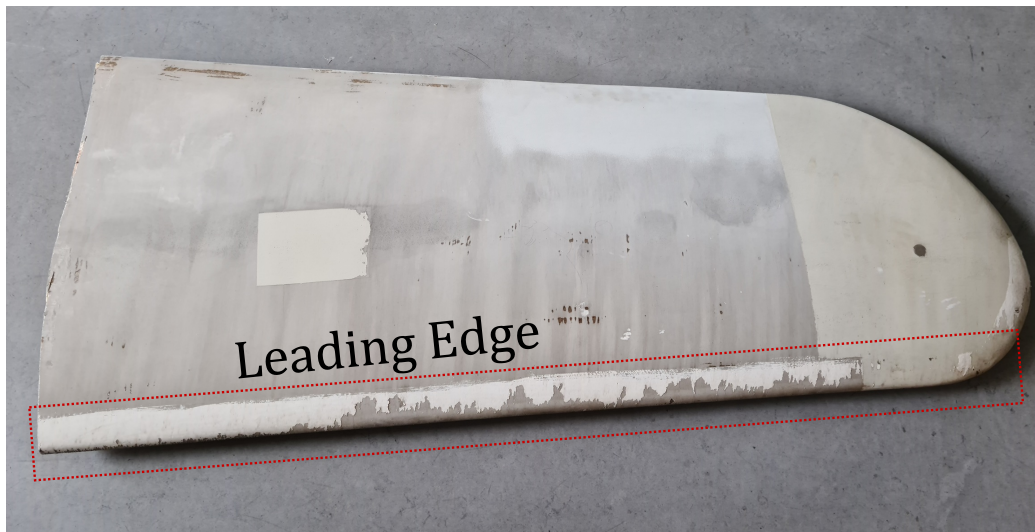


Figure 1. Rotor blade tip of a 22 year old wind turbine with a length of approx. 150 cm. The leading edge is highlighted in red.

Research has demonstrated that surface erosion, particularly that resulting from rain, sand and particle abrasion, exerts a substantial influence on operating costs (OPEX).<sup>6</sup> The inspection of a rotor blade, and if necessary, its repair, can incur expenses amounting to up to 30,000 US dollars per blade. The financial burden associated with acquiring a new rotor blade can reach up to 200,000 USD. This cost can be further increased when considering the expenses associated with its replacement.<sup>1,2</sup>

Conventional inspection methods, including visual inspections, ultrasonic tests, and manual knock tests, are characterized by several drawbacks. These methods are often time-consuming and prone to errors. This is particularly noticeable for offshore installations, where accessibility and weather conditions pose additional challenges.<sup>5</sup> For these reasons, a cost-effective but also flexible inspection is of great interest. At present, inspections carried out using camera images recorded by drones are an economically advantageous alternative compared to using human rope access methods.<sup>3</sup> Drones are particularly characterized in this type of application by their flexibility and ability to reach difficult to access locations. However, it should be noted that the generation of 2D images of the surface by the camera can lead to errors due to the lack of contrast. In order to reduce such errors and ensure more precise detection of surface anomalies, the use of 3D surface detection is required. A variety of methodologies exist for the implementation of 3D surface detection. These include tactile and depth scanning methods, which have been demonstrated to yield optimal results.<sup>8</sup> However, both methods are unsuitable for this type of application, especially in combination with a drone, due to their speed and susceptibility to noise. Fringe projection profilometry (FFP) is a promising alternative in this context. This method can be used in single-shot mode and is therefore robust against motion blur and motion-induced noise that is unavoidable with a drone.<sup>9</sup> However, it should also be noted that the noise robustness strongly depends on the evaluation algorithm.<sup>10</sup>

In addition to noise robustness, FFP is characterized by a relatively large field of view of often more than 100 cm<sup>2</sup>, which enables fast inspection even of larger surfaces.<sup>11</sup> The next section presents a detailed description of the signal formation, signal processing and a measurement setup.

## 2. PRINCIPLE

Fringe projection profilometry (FFP) is an optical, non-contact and high-resolution 3D measurement method. It is used successfully in many industries, e.g. in automotive manufacturing, medical technology or microsystems

technology, for precise surface measurement.<sup>12</sup> The method is based on the projection of a known light pattern (usually a fringe pattern) onto the surface to be examined and the subsequent analysis of the distortions in the recorded image. In this way, even microscopically small deformations, cracks or unevenness can be reconstructed in three dimensions. The projected fringe pattern can be described by the formula

$$I = I_0 (1 + V_0 \cos(2\pi x f_s + \varphi(x))), \quad (1)$$

where  $I_0$  is an intensity offset,  $V_0$  a scaling factor,  $f_s$  is the fringe frequency of the fringe image received by the camera, which can be described by the inverse of the period length of the projected grating  $T_p$ ,  $\varphi$  is the phase that represents the relationship to the height with  $\varphi(x) = 2\pi h(x) \sin(\alpha)/T_p$ .  $\alpha$  describes the triangulation angle between the projector and the camera.

Several approaches for extracting the phases and consequently the height information from Eq. (1) are known. The most common approach is the phase-shifting method. This consists of taking several images of a surface to be measured with different starting phases. Subsequently, these are converted into phase changes in the spatial domain.<sup>13</sup> As already mentioned in the motivation, this method is unsuitable for a system that is sensitive to motion, as is the case when mounted on a drone. Therefore, a single-shot method must be used. As the name suggests, the evaluation of a single-shot method is based on a single image. A variety of evaluation methods exist, which are related to the spatial frequency domain such as the Fourier transform, or to the spatial domain as the Hilbert transform, or represent a combination of both, such as the short-time Fourier transformation (STFT).<sup>12,14</sup>

### 3. SETUP AND ANALYSIS

The entire system consists of a camera with a resolution of  $2840 \times 2840$  pixels with a fixed focal length objective with a focal length of 50 mm and a static fringe projector. This system is shown in Fig. 2, with the projection system more precisely depicted on the right-hand side of the figure.

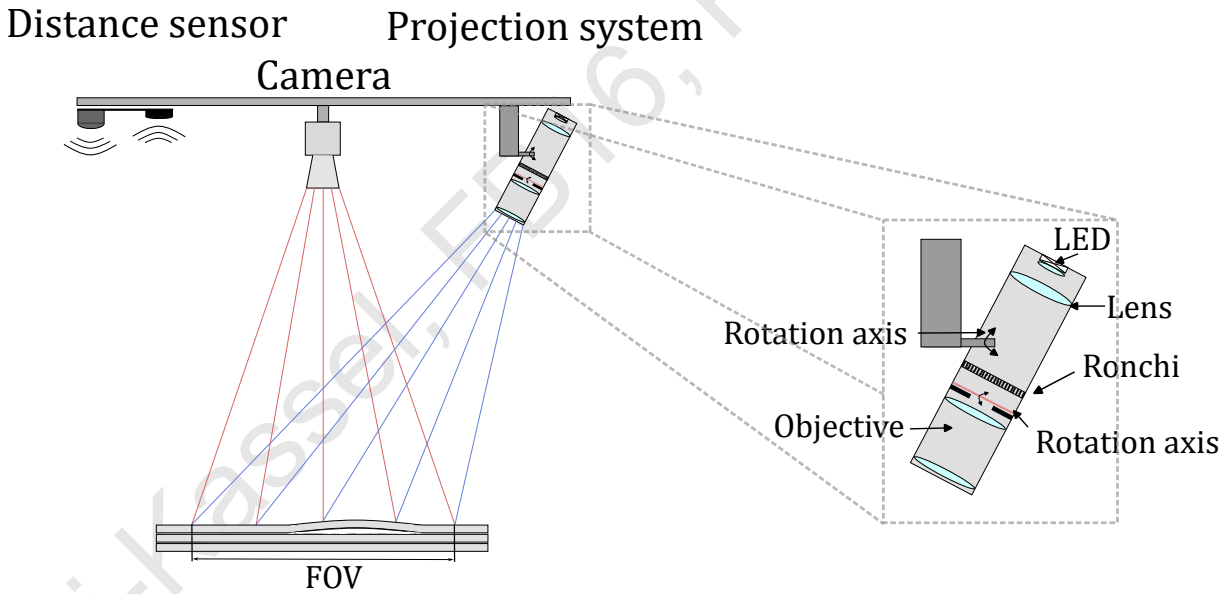


Figure 2. Setup of the fringe projection system, with a camera pointing vertically downwards. The projector, which projects a Ronchi grating onto the surface, is shown in more detail on the right. The distance sensor shown has not yet been implemented.

The distance between the camera and the projector is 300 mm, resulting in an angle  $\alpha$  of  $18^\circ$  and a field of view of the camera of  $155 \text{ mm} \times 155 \text{ mm}$  at a working distance of 1 m. The projection system consists of

an LED that focuses the light through a lens and illuminates a Ronchi transmission grating (10 LP/mm). The Ronchi grating is imaged onto the surface through a objective. The objective was designed with an axis of rotation with respect to the Ronchi grating so that the Scheimpflug condition can be fulfilled in order to achieve a sharp fringe pattern.<sup>15</sup> An alternative option to the Scheimpflug arrangement would be to increase the depth of field by reducing the aperture of the objective. However, this would result in a reduction in the light yield of the projection system. In consideration of the intended application of this system on a drone with ambient background lighting, a reduction in the light yield is problematic, so that the Scheimpflug setup is the more advantageous option. The Scheimpflug condition of a projection plane tilted towards the object to be imaged is fulfilled precisely when the imaging objective is tilted in such a way that an extension of the imaging plane, the objective and the projection plane are converging at a point of intersection. Figure 3 visualizes this concept using red dashed lines in the deployed projection system.

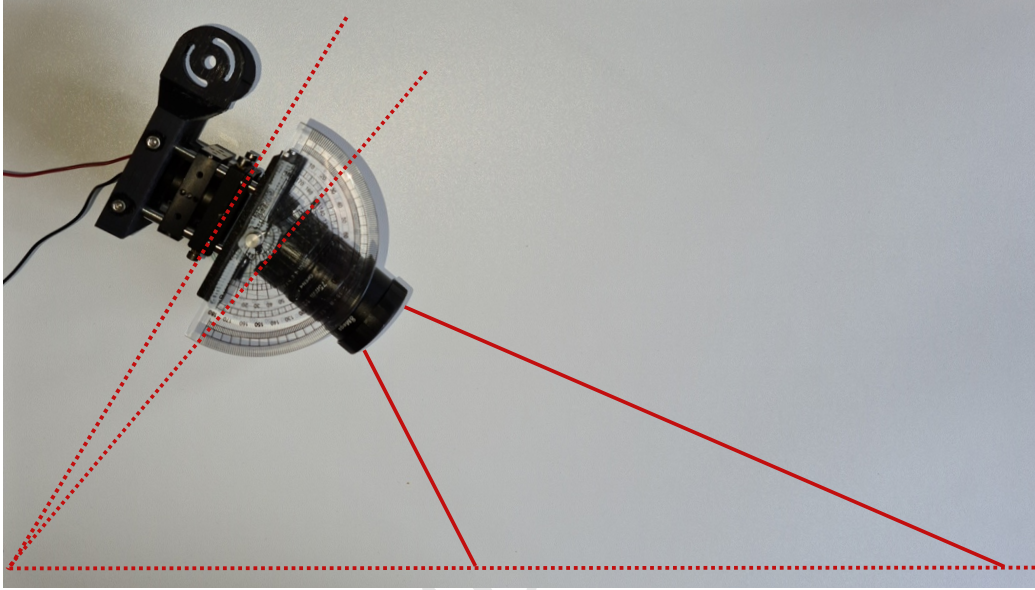


Figure 3. The projection system with the Scheimpflug condition shown in red. The angle of around 20° shown here is only used to illustrate the Scheimpflug condition.

The final complete system should also have an ultrasonic or other distance sensor, which is sketched in Fig. 2 top left to enable correct triggering of the overall system in the focus area.

Figure 4 shows a fringe pattern on a surface of a rotor blade a) and a fringe pattern on a reference b) recorded with the system introduced. This reference is a flat, white painted panel. By using the reference, errors in the projection system can be eliminated by subtracting the evaluated phases. One of these errors, which is probably due to contamination or a defect in the Ronchi grating, can be seen at approx.  $(x = 112 \text{ mm}, y = 98 \text{ mm})$ . In addition, due to the projection at an angle  $\alpha$ , the fringe frequency changes along  $x$ , which would lead to a distorted height reconstruction. This can also be corrected by subtracting the reference phase.

### 3.1 Hilbert-Transform

The Hilbert transform (HT) is a mathematical method that can be used to obtain the analytical signal. This signal can then be used to extract the local amplitude and phase of a real-valued signal. As the phase contains direct information about the height, as described in Sec. 2, this is the quantity of interest. The HT  $\mathcal{H}\{\cdot\}$  shifts the phase of a signal  $s(x)$  by 90°. In frequency space, this can be described by

$$\mathcal{H}\{s(x)\} = \hat{s}(x) = -i\mathcal{F}^{-1}\{\text{sgn}(f_x) \cdot S(f_x)\}, \quad (2)$$

where  $\mathcal{F}^{-1}\{\cdot\}$  is the inverse Fourier transform,  $S(f_x)$  is the Fourier transform of  $s(x)$ ,  $f_x$  are the spatial frequencies and  $\text{sgn}(f_x)$  is the signum function that describes the sign of the frequencies.<sup>16</sup> The HT of the

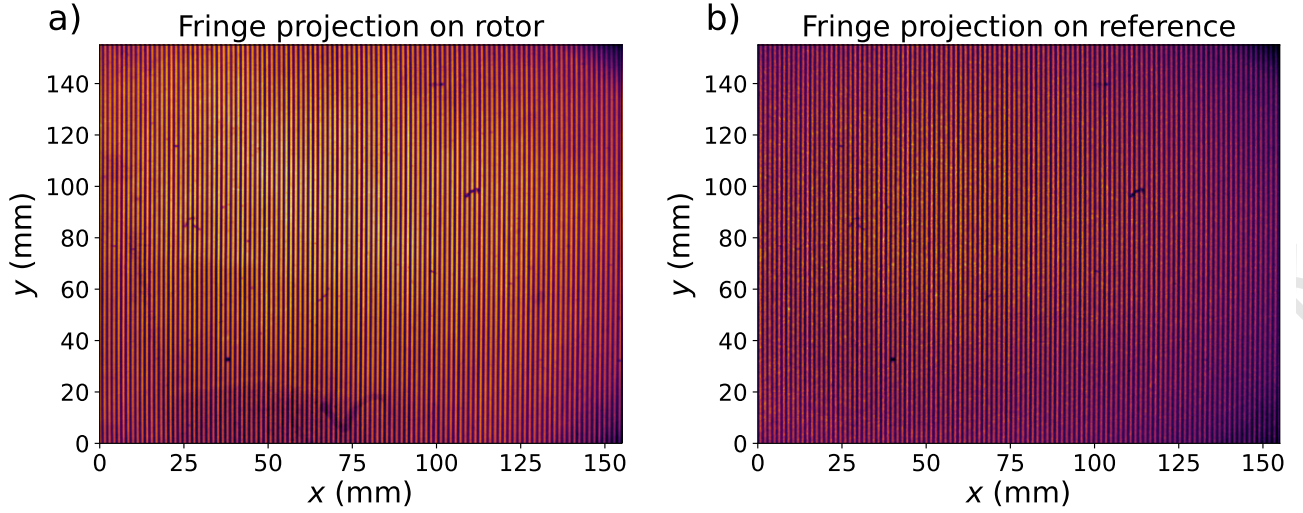


Figure 4. Camera view of a) a rotor blade surface and b) a white-painted, flat panel with projected fringes.

original signal can be combined with the original signal to form an analytical signal with  $s_a(x) = s(x) + i\hat{s}(x)$ . The local phase can be calculated directly from this complex signal with

$$\phi = \arg(s_a(x)) = \arctan\left(\frac{\Im\{s_a(x)\}}{\Re\{s_a(x)\}}\right), \quad (3)$$

where  $\Im\{\cdot\}$  and  $\Re\{\cdot\}$  describe the imaginary and real parts.<sup>17</sup> Due to the arctan function, the phase contains phase jumps of  $2\pi$  when the height exceeds the ambiguity range. The resulting phase is therefore also called wrapped phase. If there is a continuous change in height, this wrapped phase can be unwrapped so that the height can be calculated correctly.<sup>18</sup>

### 3.2 Short-Time Fourier Transform

The Short-Time Fourier Transform (STFT) is a method that analyzes the frequency content of a signal locally in the time or spatial domain.<sup>19</sup> This method extends the conventional Fourier transform by obtaining local or temporal information. In contrast to the conventional Fourier transform, which provides a global frequency spectrum, the STFT analyzes the signal locally in the spatial domain by dividing it into small sections, so-called windows. A Fourier transform is then performed within each window; this procedure is shown in Fig. 5.

A Hanning window is used as the window function, which is shifted over each row of the two-dimensional pixel image and is then multiplied by the signal. As a minimum, the window width should comprise one period length of the fringe image in order to contain adequate information. The window is shifted by a certain number of pixels at a time. The STFT can therefore be written as

$$S(\hat{x}, f_x) = \int_{-\infty}^{\infty} s(x)w(x - \hat{x})e^{-i2\pi f_x x} dx, \quad (4)$$

where  $S(\hat{x}, f_x)$  is essentially the Fourier transform of  $s(x)w(x - \hat{x})$ .<sup>20</sup>  $w$  is the window function,  $\hat{x}$  the spatial axis and  $f_x$  the spatial frequency. Thus, the STFT of a 1D signal as shown in Fig. 5 generally results in a 2D spectrum that contains information about location and spatial frequency. Since the relevant phase changes of Eq. (4) are at or near the fringe frequency  $f_s$ , it is sufficient to perform only this frequency with a locked-in type of DFT. The DFT can be calculated by

$$S(m, f_s) = \sum_{n=0}^{N-1} s[n]w[n - m] \cdot e^{-i2\pi k_s n/N}, \quad (5)$$

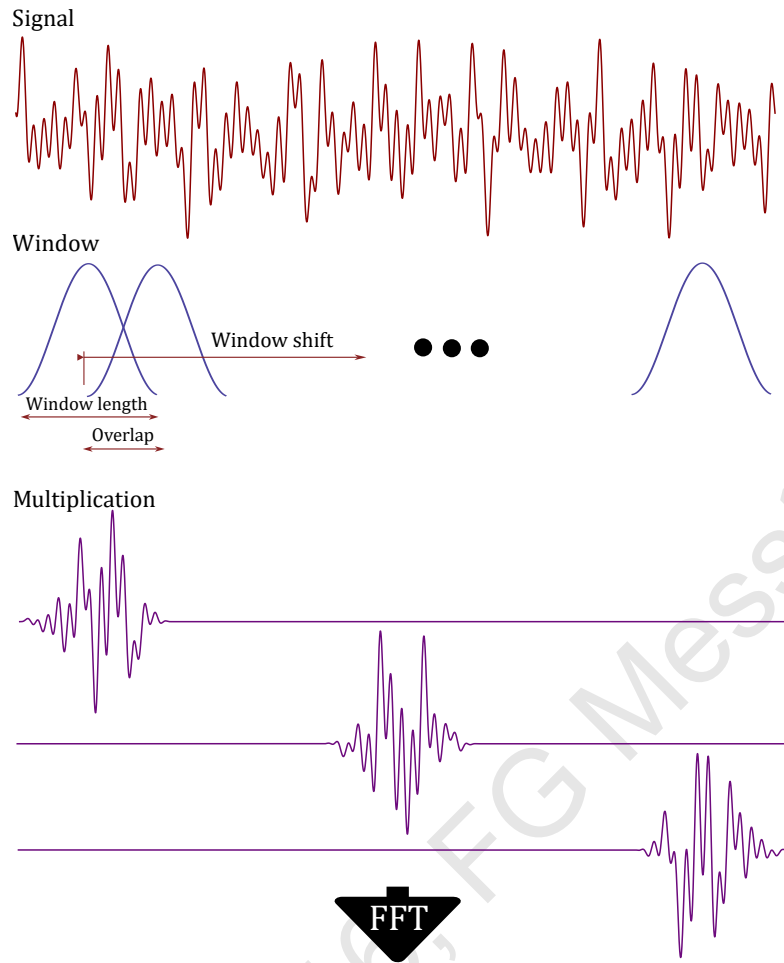


Figure 5. Schematic depiction of the evaluation of a signal using STFT. The signal is multiplied by a window function and then Fourier transformed.

where  $k_s$  is a fixed frequency sample number associated with  $f_s$  and  $N$  is the total number of frequency samples. This results in a complex number for each point of the original image, which contains information about the phase of the cosine function (Eq. (1)). The phase can be represented by the angle of the imaginary and real parts with Eq. (3).

#### 4. RESULTS

In this study, the feasibility of measuring the surface features of rotor blades using FPP is analyzed. For this purpose, three sections of a rotor blade are examined, which are shown in Fig. 6. The original surface of a 22-year-old rotor blade is shown on the left. In the center, a piece of this surface is shown that has been coated with a common matte coating and on the right with a common glossy coating for leading edges. The coating materials used were Bergolin Topcoat 6P1600 in the middle and Bergolin LEP 6D1100 on the right, both with the color standard RAL 7035. This color was chosen due to its high similarity to the original.

The reconstructed surface for the original coating is shown in Fig. 7. The surface reconstructed by HT is



Figure 6. Rotor blade sections with different coatings. On the left is a section with the original coating dating from 22 years ago, in the middle one with the Bergolin coating 6P1600 and on the right one with the Bergolin coating LEP 6D1100. The color RAL 7035 was used for both Bergolin coatings.

shown in a), the surface reconstructed by STFT is shown in b) and a section through  $x$  and  $y$  of the reconstructed surface of b) is shown in c).

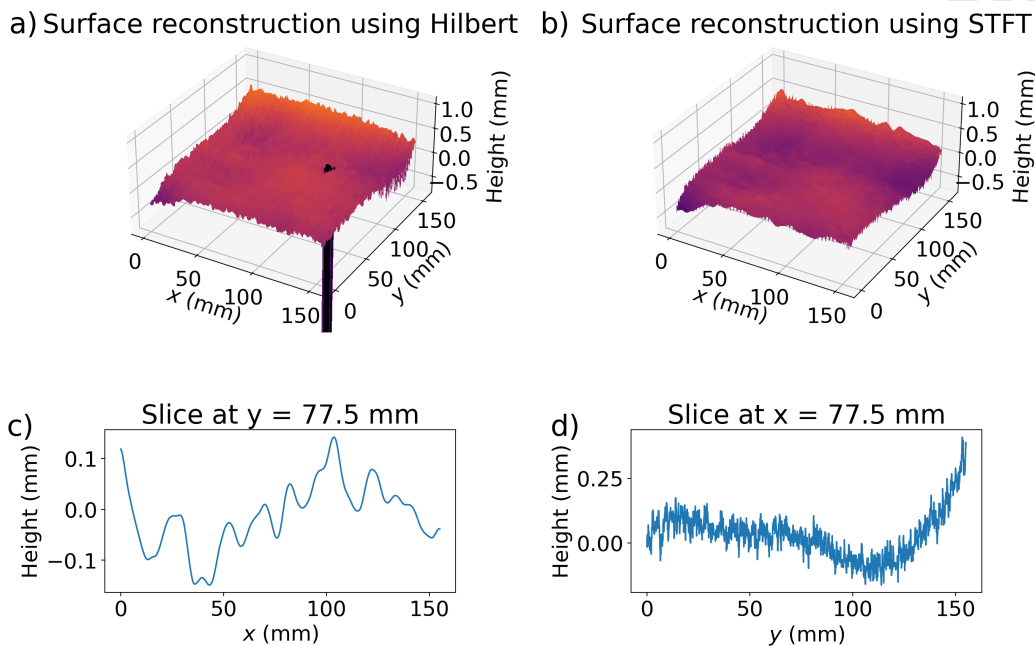


Figure 7. Surface reconstruction of a rotor blade section with 22-year-old original coating. a) Reconstructed topography using HT. b) Reconstructed topography using STFT. c) Cross-section at  $y = 77.5$  mm from the reconstruction with STFT. d) Cross-section at  $x = 77.5$  mm from the reconstruction with STFT.

The height reconstruction based on HT shows a significant anomaly at  $x = 110$  mm and  $y = 95$  mm, which is not evident either on the original surface or on the reconstructed surface using STFT. The cause of this error is most likely due to contamination of the projection system. Although this type of error should in principle be eliminated by the reference measurement, this is not guaranteed due to the sensitivity of the initial conditions in the HT. This error can generally be avoided in a laboratory setting, as the following measurements show. In the context of using drones, it is highly unlikely that this error can be avoided, which is why it is particularly emphasized here.

Figure 8 and Fig. 9 display the surface reconstruction of the rotor blade sections with the newly applied coatings. In Fig. 8 the matte coating, as seen in Fig. 6 in the center, and in Fig. 9 the glossy coating, as seen in Fig. 6 on the right, are shown.

In both cases, the surface extraction using HT shows no anomalies like those in Fig. 7. This is due to the optimal reference image, which minimizes the imaging errors of the projection system. In the evaluation

a) Surface reconstruction using Hilbert b) Surface reconstruction using STFT

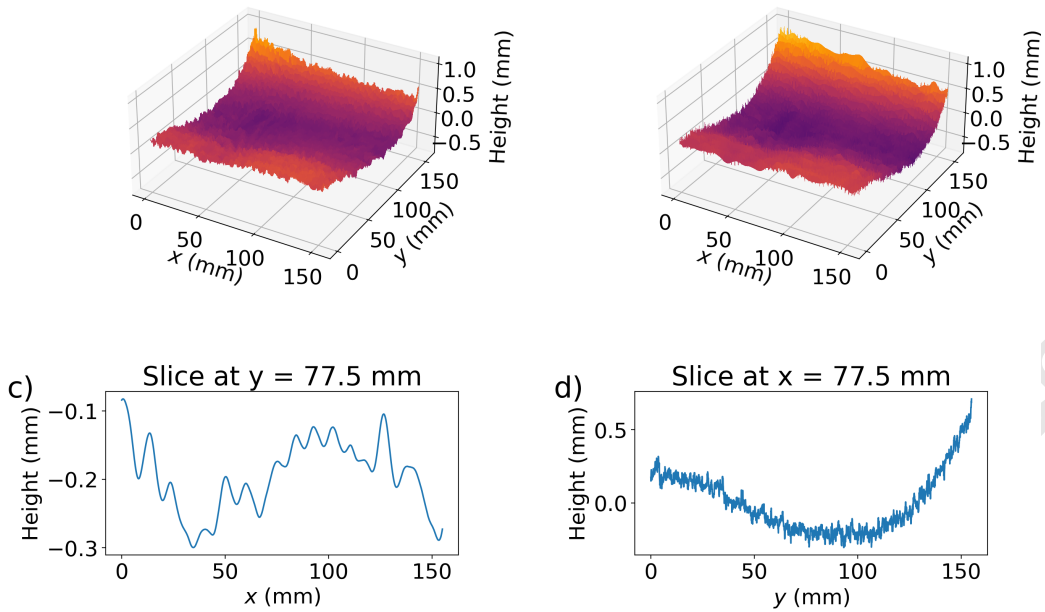


Figure 8. Surface reconstruction of a rotor blade section with matte coating. a) Reconstructed topography using HT. b) Reconstructed topography using STFT. c) Cross-section at  $y = 77.5$  mm from the reconstruction with STFT. d) Cross-section at  $x = 77.5$  mm from the reconstruction with STFT.

a) Surface reconstruction using Hilbert b) Surface reconstruction using STFT

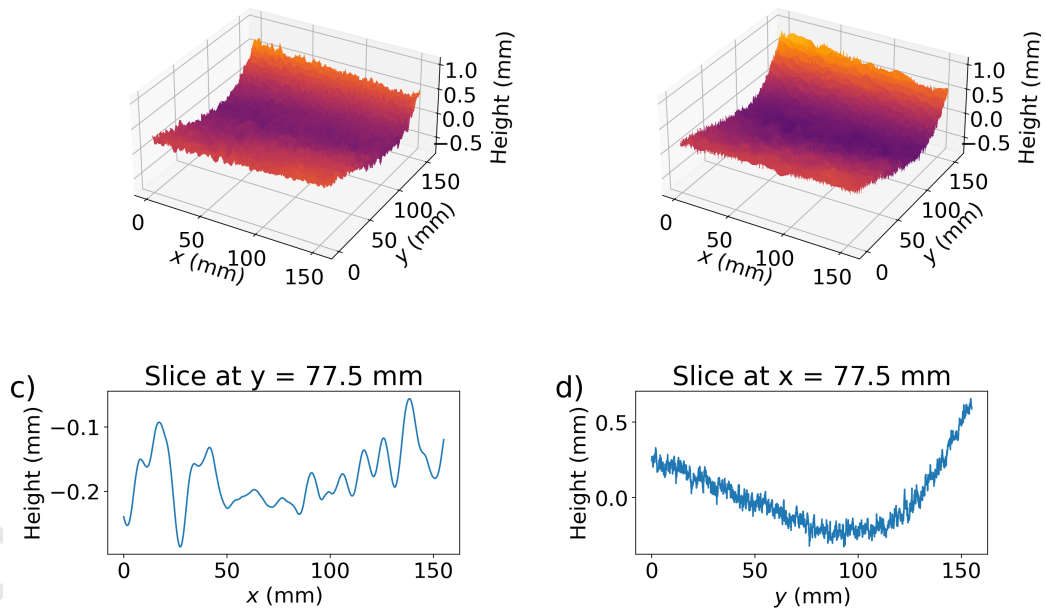


Figure 9. Surface reconstruction of a rotor blade section with glossy coating. a) Reconstructed topography using HT. b) Reconstructed topography using STFT. c) Cross-section at  $y = 77.5$  mm from the reconstruction with STFT. d) Cross-section at  $x = 77.5$  mm from the reconstruction with STFT.

with HT a slightly reduced amplitude can be seen for all three surfaces compared to the reconstruction using STFT. The reason for this is presumably the use of a median filter on the reconstructed height in the evaluation with HT. This filter comprising a sub-matrix of  $50 \times 50$  pixels is necessary to make the signal-to-noise ratio (SNR) comparable with that of the reconstructed surface using STFT. This relatively large median filter can be used because the surface is continuous. Note that reducing the sub-matrix to  $20 \times 20$  pixels results in also no significant overshoot. However, the SNR is not comparable to that of the STFT. With an optimal reference image, this filter can be reduced even further. The cross-sections along a fixed  $y$  value, which is shown in Figs. 7c), 8c) and 9c), exhibit a similar deviation of around  $200 \mu\text{m}$  for all coatings. In the cross-section along a fixed  $x$  value, which is shown respectively in Figs. 7d), 8d) and 9d), a slight improvement in the SNR of the two new coatings can be seen. This is presumably due to the smoother surface caused by the new coatings, which has not yet been exposed to environmental stress. Furthermore, it can be observed that higher-frequency noise occurs at the cross-section along  $y$  compared to the cross-section along  $x$ . This is because the STFT multiplies the signal along the fringe frequency  $x$  by a window function, thereby filtering out the high-frequency component. In contrast, there is no filtering perpendicular to the strip frequency.

## 5. CONCLUSION

This contribution discusses the need for new technologies for inspecting surfaces in difficult to access locations, such as the rotor blades of a wind turbine. For this purpose, a concept for an FPP system on a drone is presented. As part of an initial feasibility study, the system will initially be used without a drone in the laboratory to analyze rotor blade sections with different coatings. The results presented demonstrate that the analysis of these surfaces using fringe projection is suitable and that the surface therefore has the necessary reflective properties. Two evaluation algorithms are used for the analysis: the Hilbert transform and the Short-Time Fourier Transform (STFT). The STFT has proven to be significantly more robust in this context. With regard to the different coatings, there was a slight improvement in the SNR for both newly applied coatings compared to the 22-year-old original coating.

## ACKNOWLEDGMENTS

The support of this work by the Deutsche Forschungsgemeinschaft (DFG, LE 992/19-1) is gratefully acknowledged.

## REFERENCES

- [1] Mishnaevsky, L., "Root causes and mechanisms of failure of wind turbine blades: Overview," *Materials* **15**(9), 2959 (2022).
- [2] Mishnaevsky, L., "Repair of wind turbine blades: Review of methods and related computational mechanics problems," *Renewable energy* **140**, 828–839 (2019).
- [3] Yang, C., Liu, X., Zhou, H., Ke, Y., and See, J., "Towards accurate image stitching for drone-based wind turbine blade inspection," *Renewable Energy* **203**, 267–279 (2023).
- [4] Amenabar, I., Mendikute, A., López-Arraiza, A., Lizaranzu, M., and Aurrekoetxea, J., "Comparison and analysis of non-destructive testing techniques suitable for delamination inspection in wind turbine blades," *Composites Part B: Engineering* **42**(5), 1298–1305 (2011).
- [5] Hayman, B., Wedel-Heinen, J., and Brøndsted, P., "Materials challenges in present and future wind energy," *MRS bulletin* **33**(4), 343–353 (2008).
- [6] Mishnaevsky, L. and Thomsen, K., "Costs of repair of wind turbine blades: Influence of technology aspects," *Wind Energy* **23**(12), 2247–2255 (2020).
- [7] Remmers, J. and De Borst, R., "Delamination buckling of fibre–metal laminates," *Composites Science and Technology* **61**(15), 2207–2213 (2001).
- [8] Hagemeyer, S., *Comparison and investigation of various topography sensors using a multisensor measuring system*, PhD thesis, Universität Kassel (2022).
- [9] Zhang, Z., "Review of single-shot 3D shape measurement by phase calculation-based fringe projection techniques," *Optics and lasers in engineering* **50**(8), 1097–1106 (2012).

- [10] Quan, C., Chen, W., and Tay, C., "Phase-retrieval techniques in fringe-projection profilometry," *Optics and Lasers in Engineering* **48**(2), 235–243 (2010).
- [11] Keferstein, C. P. and Dutschke, W., [*Fertigungsmesstechnik*], Springer (2010).
- [12] Gorthi, S. S. and Rastogi, P., "Fringe projection techniques: whither we are?," *Optics and Lasers in Engineering* **48**(2), 133–140 (2010).
- [13] Zuo, C., Feng, S., Huang, L., Tao, T., Yin, W., and Chen, Q., "Phase shifting algorithms for fringe projection profilometry: A review," *Optics and lasers in engineering* **109**, 23–59 (2018).
- [14] Kemaq, Q., "Windowed fourier transform for fringe pattern analysis," *Applied Optics* **43**(13), 2695–2702 (2004).
- [15] Albers, O., Poesch, A., and Reithmeier, E., "Flexible calibration and measurement strategy for a multi-sensor fringe projection unit," *Optics express* **23**(23), 29592–29607 (2015).
- [16] King, F. W., [*Hilbert Transforms*], Encyclopedia of Mathematics and its Applications, Cambridge University Press (2009).
- [17] Xu, J. and Zhang, S., "Status, challenges, and future perspectives of fringe projection profilometry," *Optics and Lasers in Engineering* **135**, 106193 (2020).
- [18] Herráez, M. A., Burton, D. R., Lalor, M. J., and Gdeisat, M. A., "Fast two-dimensional phase-unwrapping algorithm based on sorting by reliability following a noncontinuous path," *Applied optics* **41**(35), 7437–7444 (2002).
- [19] Gröchenig, K., [*Foundations of time-frequency analysis*], Springer Science & Business Media (2001).
- [20] Cordero, E. and Rodino, L., [*Time-frequency analysis of operators*], vol. 75, Walter de Gruyter GmbH & Co KG (2020).

J. Riebeling, G. Ehret, P. Lehmann, "Optical form measurement system using a line-scan interferometer and distance measuring interferometers for run-out compensation of the rotational object stage" SPIE Proceedings 11056, Optical Measurement Systems for Industrial Inspection XI, 110562D, (June 21, 2019).

<https://doi.org/10.1117/12.3062548>

Copyright 2025, Society of Photo-Optical Instrumentation Engineers (SPIE). One print or electronic copy may be made for personal use only. Systematic reproduction and distribution, duplication of any material in this paper for a fee or for commercial purposes, or modification of the content of the paper are prohibited.